Biofilm Interaction Mapping and Analysis (BIMA): A tool for deconstructing interspecific interactions in co-culture biofilms

Suzanne M. Kosina[a], Peter Rademacher[a*], Kelly M. Wetmore[a], Markus de Raad[a], Marcin Zemla[a*], Grant M. Zane[b], Jennifer J. Zulovich[b], Romy Chakraborty[a], Benjamin P. Bowen[a,c], Judy D. Wall[b], Manfred Auer[a], Adam P. Arkin, Adam M. Deutschbauer[a], Trent R. Northen[a,c#]

[a]Environmental Genomics and Systems Biology, Lawrence Berkeley National Laboratory, Berkeley, CA, USA

[b]University of Missouri, Department of Biochemistry, Columbia, MO 65211, USA

[c]Joint Genome Institute, Lawrence Berkeley National Laboratory, Berkeley, CA 94720, USA

#Corresponding Author: email: trnorthen@lbl.gov

*Current addresses: P. Rademacher – DiCe Molecules, South San Francisco, CA; M. Zemla - Thermo Fisher Scientific, Hillsboro, OR.

ABSTRACT

Pseudomonas species are ubiquitous in nature and include numerous medically, agriculturally and technologically beneficial strains of which the interspecific interactions are of great interest for biotechnologies. Specifically, co-cultures containing *Pseudomonas stutzeri* have been used for bioremediation, biocontrol, aquaculture management and wastewater denitrification. Furthermore, the use of *P. stutzeri* biofilms, in combination with consortia based approaches, may offer advantages for these processes. Understanding the interspecific interaction within biofilm co-cultures or consortia provides a means for improvement of current technologies. However, the investigation of biofilm based consortia has been limited. We present an adaptable and scalable method for the analysis of macroscopic interactions (colony morphology, inhibition and invasion) between colony forming bacterial strains using an automated printing method followed by analysis of the genes and metabolites involved

in the interactions. Using Biofilm Interaction Mapping and Analysis (BIMA), these interactions were investigated between *P. stutzeri* strain RCH2, a denitrifier isolated from chromium (VI) contaminated soil, and thirteen other species of pseudomonas isolated from non-contaminated soil. The metabolites and genes associated with both active co-culture growth and inhibitory growth were investigated using mass spectrometry based metabolomics and mutant fitness profiling of a DNA-barcoded mutant library. One interaction partner, Pseudomonas fluorescens N1B4 was selected for mutant fitness profiling; with this approach four genes of importance were identified and the effects on interactions were evaluated with deletion mutants and metabolomics.

IMPORTANCE

The Biofilm Interaction Mapping and Analysis (BIMA) methodology provides a way to rapidly screen for positive and negative interspecific interactions, followed by an analysis of the genes and metabolites that may be involved. Knowledge of these may offer opportunities for engineered strains with improved function in biotechnology systems. *P. stutzeri*, an organism with wide-spread utilization in consortia based biotechnologies, was used to demonstrate the utility of this approach. Where little is known about the factors influencing biofilm based interactions, elucidation of the genes and metabolites involved allows for better control of the system for improved function or yield.

INTRODUCTION

Consortia based systems in biotechnologies are widespread, however controlling them is challenging due to the genomic and metabolomic complexities of the interactions. Characterization of the genes and metabolites involved in the interactions opens up the possibility for improved consortia functionality by use of engineered strains and culture condition metabolite amendments. Previously, metabolomics of adjacently printed cultures of *P. stutzeri* and *Shewanella oneidensis* were analyzed using replication-exchange-transfer and nanostructure initiator mass spectrometry; however this

47 approach does not elucidate the genes important for the interactions (1). The ability to incorporate
48 genomics into these types of approaches will allow for a better understanding of the interactions
49 involved. Barcoded mutant libraries are proving to be a powerful tool for the discovery of the genetic
50 determinants of co-culture fitness (2, 3). Next-generation sequencing enables rapid profiling of the
51 abundance of barcodes mapped to specific genes in transposon mutant libraries under a wide range of
52 environmental conditions (4, 5) and when integrated with metabolomics, provides rapid functional
53 assignment of transport and metabolic processes (6) important in microbial interactions.

54

55 Pseudomonas are a diverse genus of microbes that have been isolated from all over the world of which
56 both beneficial and pathogenic strains have been identified (7, 8). As common soil dwelling
57 microorganisms, they are important constituents of microbial ecosystems and rhizosphere
58 environments (9–12). *Pseudomonas stutzeri*, a model denitrifying pseudomonas, can grow in diverse
59 conditions (13) and its use has been demonstrated in a number of bioremediation processes, including
60 phenol (14), carbon tetrachloride (15), uranium (16), polycyclic aromatic hydrocarbons (17) and diesel
61 oil (18). Additionally, *P. stutzeri* has been discovered and used in a number of consortia based
62 applications, such as bioremediation (19–21), wastewater denitrification (22, 23), aquaculture water
63 quality management (24, 25), as a plant growth promoter for the biocontrol of phytopathogens (26, 27)
64 and manufacturing/municipal waste management (28, 29). The use of *P. stutzeri* biofilms for various
65 bioremediation efforts has potential benefits in terms of activity and yields for copper removal (30),
66 drinking water denitrification (31) and naphthalene (32) and phenol (33) degradation. Given this
67 widespread utilization in both microbial consortia systems and biofilms, *P. stutzeri* was selected to
68 demonstrate the deconstruction of its interactions with other pseudomonas in biofilm-based co-cultures
69 into the genetic and chemical aspects influencing the co-colony fitness.

Here we introduce Biofilm Interaction Mapping and Analysis (BIMA), an integrated platform of automated colony printing, barcoded mutant library profiling and metabolomics to discover and deconstruct the interactions within biofilm-based consortia (Fig. 1). Overlaid colonies were printed using an automated liquid handling system to investigate the morphological, inhibitory and invasive interactions between *P. stutzeri* and other pseudomonas soil isolates in a lab model for a biofilm based consortia. The overlaid colonies were further analyzed using transmission electron microscopy to investigate changes to the species interface over time. Using a DNA-barcoded mutant transposon library of *P. stuzeri* strain RCH2, we identified genes associated with the fitness of the RCH2 in the co-colony. Additionally, exometabolomic analysis was used to evaluate the exchange of metabolites between RCH2 and another pseudomonas strain. We foresee these tools being valuable resources for both the understanding of natural interactions between pseudomonas in microbial communities and in the development of biofilm based biotechnological applications.

MATERIALS AND METHODS

Bacterial strains and growth conditions. *Pseudomonas stutzeri* RCH2 was isolated from chromium(VI) contaminated groundwater at the Department of Energy Hanford 100 Area, Benton County, WA (34). Thirteen additional pseudomonas strains were isolated from Oak Ridge National Laboratory, Field Research Center, TN under conditions indicated in Supplemental table S1. Liquid cultures were inoculated into 3-(N-morpholino)propanesulfonic acid (MOPS) buffered casein yeast magnesium broth (Mb-CYM): 10 g/L pancreatic digest of casein, 5 g/L Difco yeast extract, 1 g/L $MgSO_4$ heptahydrate, 10 mM MOPS. Mb-CYM agar was prepared with the addition of 1.5% w/v of agar. Unless otherwise noted, culture conditions were as follows. Strains were maintained as glycerol stocks; revived cultures were plated onto agar plates, incubated at 30°C for 24 hours and stored at 4°C. Starter cultures for experiments were prepared from single colonies inoculated into liquid Mb-CYM broth and cultured aerobically with shaking at 30°C overnight. Uninoculated and unstreaked but incubated cultures/plates

were used as negative controls for contamination. In figures and text, *Pseudomonas stutzeri* RCH2 is referred to as culture #1, while the thirteen other strains are referred to as cultures #2-14, and uninoculated controls as culture #15 as indicated in Supplemental Table SI.

Printed colony biofilm morphology screening assay

Rectangular petri dishes with ANSI standard dimensions were poured with agar to a height of 5 mm. Overnight cultures of the fourteen effector strains (including RCH2) and uninoculated control broth (Supplemental table S1) were diluted 1:50 in fresh Mb-MYM and then added to a 96-well plate. The plates were loaded onto a Hamilton Vantage Liquid Handling System equipped with a 96 pipetting head which was used to dip pipette tips into the liquid cultures and press/print them against the surface of the agar in a grid; a single colony of each unique strain was printed in a 3 x 5 grid (Fig. 2A). The lidded-plate was sealed with Parafilm and incubated at 30^{o}C for two days once visible colonies had formed of similar size (Supplemental figure S1). Printing was repeated using only *P. stutzeri* RCH2 (the interaction strain) in all well positions of a 16 x 24 grid (ANSI standard dimensions of a 384 well plate), excluding the positions from the original print at time 0 (Fig. 2A). Cultures were incubated for an additional 4 days prior to imaging using a digital camera. Image analysis was performed using ImageJ (35). Briefly, the image was converted to 16-bit grayscale, corrected for uneven lighting using the FFT bandpass filter (filter large structures to 70 pixels and small structures to 5 pixels, 5% tolerance, autoscale and saturate after filtering), auto thresholded to black and white, and then the colonies were measured using the Analyze Particles tool (colonies missed by the automated selection were manually outlined and then measured). Measurements included area and position. Colony areas of surrounding (8 colonies in a square around the center interaction colony) and closest/farthest neighbors (sides/corners of the

116 square) were compared with the colonies surrounding the control uninoculated position (#15) using
117 Dunnett's multiple comparison procedure using R version 3.6.2 (36, 37).

118 **Co-colony overlay morphology with light microscopy and transmission electron microscopy**

119 Overnight culture of *Pseudomonas* sp. FW300-N1B4 (N1B4) was manually pipetted (10 uL) onto an agar
120 plate and incubated at 30°C overnight. Overnight culture of *P. stutzeri* RCH2 was manually pipetted (10
121 uL) over the top of the N1B4 colony with care to not puncture the colony surface and to avoid allowing
122 the droplet to spill over the sides. For time course analysis of macroscopic morphology, the rim of the
123 petri dish was sealed with parafilm and placed on a black velvet cloth under a Leica M165FC microscope
124 with a Planapo 1.0 x objective lens. Images were acquired every 2 minutes for a 24 hour period with a
125 Leica DFC400 1.4 megapixel ccd sensor digital camera set at a 9 mm frame width. For microscopic
126 colony interface analysis, after overnight growth of the overlay, the colony and underlying agar was cut
127 out from the plate and fixed for 2 hours with 2.5% glutaraldehyde in 0.1 M sodium cacodylate buffer (pH
128 7.2). Fixed samples were stained with 5 mM ruthenium red in 0.1 M sodium cacodylate buffer (pH 7.2)
129 for 1 hour and post-fixed with 1% osmium tetroxide for 1 hour. Following staining, samples were
130 dehydrated through a graded ethanol series (20%, 40%, 60%, 80%, 90%, 100%, 100%, 100%) followed by
131 infiltration with an Embed-812 epoxy resin (Electron Microscopy Sciences):acetone series of 1:3 for 2
132 hours, 2:3 for 2 hours, and 100% resin overnight. Samples were then heat polymerized in 100% resin
133 with N,N-dimethylbenzylamine accelerant for 2 hours at 85°C. 100 nm sections were cut and sectioned
134 using a Leica UC6 Ultra Microtome (Leica Microsystems Inc., Buffalo Grove, IL, USA) and then stained
135 sequentially with 2% methanolic uranyl acetate and Reynolds' lead citrate for 5 minutes each. Images
136 were collected using a FEI Tecnai 12 transmission electron microscope (FEI Company, Hillsboro, OR,
137 USA).

138 **Fitness profiling of RCH2 mutants in the presence of other pseudomonads**

The construction of the *P. stutzeri* RCH2 DNA-barcoded transposon mutant was previously described (4). Overnight culture of *Pseudomonas* sp. FW300-N1B4 was manually pipetted (10 uL) in triplicate onto LB agar plates. The plates were incubated overnight and then 5 uL of the *P. stutzeri* RCH2 barcoded transposon mutant library (in LB media) starter culture at an OD_{600} of 0.9 was spotted as overlay colonies on top of the three replicates of the underlay colonies. An aliquot of the starter culture was used for the initial RCH2 mutant abundances. Colonies were then carefully scraped and frozen for storage and subsequent analysis of the final *P. stutzeri* RCH2 mutant abundances. Gene fitness scores were calculated by comparing the initial and final mutant abundances as determined by deep sequencing of the DNA barcodes, as previously described (4).

Mutant construction

The four mutants from the pooled fitness assay with the largest absolute differential fitness where fitness of RCH2 with N1B4 was less than fitness of RCH2 on agar alone were selected for constructing gene deletion mutant strains. Deletion mutants (Supplemental table S2) for gamma-glutamyl phosphate reductase, OHCU decarboxylase, formyltetrahydrofolate deformylase and glutamate 5-kinase were constructed by conjugation of unstable, marker-exchange plasmids into *P. stutzeri* RCH2, as previously described (38) with modifications as follows. All plasmids and primers (IDT, Newark, NJ) used are listed in Supplemental tables S3 and S4, respectively. Briefly, deletion cassettes, containing kanamycin resistance gene (npt) flanked by chromosomal regions up and downstream of the gene to be deleted, were assembled using the “gene SOEing” technique (39). Cloned homologous regions were sequenced at the DNA core facility at the University of Missouri, Columbia, and compared with the published sequence for *P. stutzeri* RCH2 (40). Cassettes and the template plasmid pM07704 were amplified by polymerase chain reaction (PCR) with Herculase II DNA polymerase (Stratagene). Marker-exchange plasmids were generated by ligation of the PCR products in α-select cells (Bioline) using the SLIC cloning

method (41). The plasmids were isolated and transformed into *E. coli* strain WM3064, and then transferred to RCH2 via conjugation (42). The plasmids, containing up/downstream chromosomal regions flanking npt, allow for exchange of npt with the gene of interest in RCH2 via double homologous recombination. Exconjugates were selected on 50 ug/mL kanamycin solid medium, then screened for spectinomycin (100ug/mL) sensitivity to ensure no single recombination isolates were selected. Deletion strains were confirmed by Southern blot analysis. One isolate for each deletion of interest was retained while the other isolates were discarded. All strains were frozen as early stationary phase cultures in 10% (v/v) glycerol. RCH2 mutants used for experiments were maintained in Mb-CYM broth or Mb-CYM agar with 50 ug/mL kanamycin sulfate.

Mutant co-colony morphology analysis

Overnight cultures of RCH2 (wild-type and mutants) and N1B4 (500uL) were centrifuged (5000xg x 3min at RT) to collect cells, then washed 2 times in DPBS (resuspension in 500uL DPBS, centrifugation at 5000xg x 3 min at RT) with final resuspension adjusted to an OD (600nm, 1cm) of 0.5. Uninoculated control medium was washed and resuspended in a similar manner to account for carryover of nutrients from tube surfaces and residual volumes. Cultures ("underlays") were manually spotted (2 uL) onto Mb-CYM agar plates in a 7 x 7 format and incubated overnight at 30°C. Fresh cultures were inoculated from agar stock plates into Mb-CYM. Overlay colonies were diluted and washed in the same manner as for the underlays and then carefully spotted on top of the underlay colonies. Images were taken using a digital camera of whole plates and through a LEICA M165 FC stereo microscope (2x objective) at 24 hours (0 hours of overlays), 48 hours (24 hours of overlays), 72 hours (48 hours of overlays). Morphological differences were visually evaluated.

Metabolomics analysis

Wild-type and mutant strains of *P. stutzeri* RCH2 were cultured in 'spent' N1B4 medium (sterile filtered N1B4 culture supernatant) in liquid culture and then exometabolites were collected for LCMS analysis. For collection of 'spent' medium, overnight liquid cultures of RCH2 wild-type, RCH2 mutants, and N1B4 wild-type and uninoculated control medium were centrifuged (3000 x g x 10 minutes) to pellet cells. Supernatants were sterile filtered (0.22 um), supplemented with 1x Wolfe's vitamins and minerals (ATCC) and stored at 4°C overnight. Additional overnight cultures were diluted, washed and adjusted as described above for mutant co-colony morphology analysis, except the final OD was adjusted to 0.12 in DPBS, 20 uL of which was added to 100 uL of spent medium in 96 well plates. Cultures were prepared in triplicates for all combinations of mutants and wild-type RCH2 on spent N1B4 and fresh Mb-CYM and for N1B4 on all combinations of spent mutants and wild-type RCH2 and fresh Mb-CYM; uninoculated controls were included for each spent medium and positive growth controls were included for each strain on fresh (non-spent) medium. Cultures were incubated for 20 hours in a BioTek plate reader with OD readings taken every 30 minutes at 600nm. Cross-feeding medium from the culture was then collected via centrifugation (3000x g for 5 minutes), transferred to a new plate that was sealed with heated foil (4titude), and frozen at -80°C. Holes were pierced in the foil with an 18 gauge needle and then supernatants were lyophilized to dryness. Dried material was resuspended in 200 uL of internal standard mix (15uM 13C, 15N amino acid mix, 10 ug/mL 13C-mannitol, 13C-trehalose and 2 uM 15N4-inosine, 15N5-adenine, 13C4-15N2-uracil, 15N4-hypoxanthine, 13C4-15N2-thymine) in LCMS grade methanol, resealed, vortexed, sonicated in a room temperature water bath for 10 minutes, rechilled at -80°C for 5 minutes, and centrifuged 3000x g for 5 minutes to pellet insoluble material. Supernatants were filtered (0.22µm, PVDF) using an Apricot positive pressure filtration device. Filtrates were then arrayed into 50uL aliquots in a 384 well plate for LCMS analysis.

LCMS analysis of exometabolites from spent media fed cultures.

Extracts of polar metabolites were analyzed using hydrophilic interaction chromatography - mass spectrometry. Metabolites were retained and separated on an InfinityLab Poroshell 120 HILIC-Z column (Agilent, 683775-924, 2.7µm, 150 x 2.1 mm) using an Agilent 1290 UHPLC. Samples, held at 4°C, were injected at 4uL each; the column temperature was held at 40°C and flow rate was held at a constant 0.45mL/min. Following injection, a gradient of mobile phase A (5mM ammonium acetate, 0.2% acetic acid, 5uM methylene di-phosphonic acid in water) and mobile phase B (5mM ammonium acetate, 0.2% acetic acid in 95:5 (v/v) acetonitrile:water) was applied as follows: initial equilibration at 100% B for 1.0 minutes, linear decrease to 89% B over 10 minutes, linear decrease to 70% B over 4.75 min, linear decrease to 20% B over 0.5 min, hold at 20% B for 2.25 min, linear increase to 100% B over 0.1 min, re-equilibration at 100% B for 2.4 min. Eluted metabolites were subjected to mass spectrometry analysis on a Q Exactive Hybrid Quadrupole-Orbitrap Mass Spectrometer (Thermo Scientific) equipped with a HESI-II source probe using Full MS with Data Dependent tandem MS. Source settings were as follows: sheath gas at 55 (arbitrary units), aux gas flow at 20, sweep gas at 2, spray voltage at 3 |kV| spray, capillary temperature at 400C, and S-lens RF at 50. MS1 was set at 70,000 mass resolution, with automatic gain control target at 3.0E06 with a maximum allowed injection time of 100 milliseconds, at a 70-1050 m/z scan range. dd-MS2 was set at 17,500 mass resolution with automatic gain control target at 1.0E5 and a maximum allowed injection time of 50 milliseconds, a 2 m/z isolation window and stepped normalized collision energies at 10, 20 and 30 (dimensionless units). All data was collected in centroid mode. The scan cycle included a single MS1 scan followed by sequential MS/MS of the top two most intense MS1 ions excluding any fragmented within the previous 10 seconds. Ions selected for fragmentation must meet a minimum AGC target threshold of 1.0E3 with absolute charge less than four. Each sample was analyzed in negative ionization mode. Sample were injected in randomized order with solvent blank injections between each; internal and external standards were used for quality control purposes and for retention time predictions of compounds from in an in-house standards library. Using

custom python scripts and metabolite atlases (43, 44), mass-to-charge ratios, retention times and where possible spectra fragmentation patterns were used to confirm metabolite identification by comparison to metabolite standards analyzed using the same LC-MS/MS methods. Mutant and RCH2 cultures on N1B4 medium were compared with uninoculated control N1B4 spent medium using ANOVA and Tukey HSD in R.

Data Availability

Raw LCMS data are available from the JGI Genome Portal (genome.jgi.doe.gov) under project number 1278333.

Results

BIMA screening: Microbial interaction mapping and strain selection.

As the first step of BIMA, a colony printing method was developed on an automated liquid handling system for the purpose of scalability and transferability between labs. Fourteen preprinted 'effector' Pseudomonas strains (including RCH2) were evaluated for their effect on the growth of subsequently printed neighboring colonies of *P. stutzeri* RCH2 (Fig. 2A and 2B). Pseudomonas strains 3-9, and 11 inhibited the growth of the four closest RCH2 colonies, located along the sides of the square of neighboring colonies (Fig. 2C). Interestingly, for a subset of these (3, 4, 5), the more distant RCH2 colonies at the corners of the square of neighboring colonies had larger mean areas (Fig. 2D). Pseudomonas strain 2 (*Pseudomonas fluorescens* FW300-N1B4) was the only strain that did not inhibit RCH2 (closest side colonies) and enhanced the growth of RCH2 (corner colonies). This strain 'N1B4', was selected for further analysis in co-culture with *P. stutzeri* RCH2.

BIMA morphology: Co-colony structure and infiltration. Time lapse images of the RCH2 overlay on N1B4 were taken to evaluate the co-colony morphology. Highly wrinkled, rugose colony morphology had formed by 12 hours after application of the RCH2 overlay (Fig. 3A). The co-colony species interface was further examined using transmission electron microscopy (TEM) (Fig. 3B). TEM after 2 hours showed a stratification with a clear distinction between RCH2 on the surface and N1B4 underneath. Over the course of 24 hours, the colonies became more mixed with infiltration of the N1B4 layer by RCH2. In both the co-culture and in isolate culture, RCH2 biofilm developed exopolysaccharide sacs containing groups of spherical cells at the air interface; whereas when spotted on the surface of N1B4, single, elongated RCH2 are observed at the N1B4 interface. The sacs became visible in the 24 hour co-colony images and are similar to those observed in other *P. stutzeri* strains where the sacs are associated with oxygen exclusion for nitrogen fixation under aerobic conditions (45). The anaerobic co-colony culture developed a compact RCH2 layer with no visible EPS sacs.

BIMA genomics: Mutant fitness analysis and interactions

A pooled mutant fitness assay was used to identify RCH2 genes essential for successful co-culture growth with N1B4. The top four genes with the largest differential gene fitness between RCH2 on LB and RCH2 on N1B4, where fitness on N1B4 was negative included gamma-glutamyl phosphate reductase (*proA*), OHCU decarboxylase (*uraD*), formyltetrahydrofolate deformylase (*purU*), and glutamate 5-kinase (*proB*) (Fig 4A). To investigate these genes further, we constructed isogenic single-gene deletion strains for all four genes.

In liquid culture, while all mutants were capable of growth on fresh medium, only the *ΔuraD* deletion strain had similar growth to the wild-type when cultured on spent N1B4 medium (Fig. 4B). Minimal to no growth was observed for the *ΔproA* and *ΔproB* deletion mutants, and delayed growth was observed for the *ΔpurU* deletion mutant. N1B4 had similar growth on the spent medium of RCH2 wild-type and

mutants (not shown). The limited or delayed growth indicated these mutants were unable to acquire some required metabolite from the medium that was consumed by N1B4 in liquid culture or that growth may have been inhibited by something N1B4 was producing.

The biofilm interactions were analyzed by manual printing of the RCH2 wild-type and mutant strains on the top of an established N1B4 colony. The overlays were imaged at 24 hours and 48 hours after overlay printing (Fig. 4C). Wild-type RCH2, and *ΔproA* and *ΔuraD* deletion strains formed rugose co-colony biofilms after 24 hours similar to the wild-type but with a smoother center for *ΔproA*, while the *ΔpurU* mutant had delayed rugose formation and the *ΔproB* mutant remained smooth up to 72 hours of observation. All mutants formed rugose colonies after 24 hours of overlay on control medium. On its own, the *ΔpurD* formed more tubular structures than the wild-type alone, similar to growth on N1B4 for both (Supplemental Fig. S3).

BIMA metabolomics: Potential for metabolite exchange

To further evaluate why the four RCH2 genes identified in the mutant fitness assay were important to growth in the co-colony, spent medium from N1B4 was fed to each of the mutants and the wild-type RCH2 and then metabolomics was performed to check for altered metabolism in the mutants. Despite limited growth of three of the mutants on N1B4 spent medium (Fig. 4B), all four RCH2 mutants appeared to be metabolically active with significant increases and decreases in metabolite abundances relative to uninoculated N1B4 spent medium and in many cases were significantly different than the wild-type (Fig 5 and Supplemental Fig. S4). Metabolites in pathways associated with the mutated genes, including one-carbon (C1) metabolism (PurU), ureide pathway (UraD) and proline synthesis (ProA/B) were evaluated further (Supplemental Fig. S05). The *P. stutzeri* RCH2 wildtype consumed several N1B4 metabolites involved in one-carbon (C1) metabolism though consumption of methionine was reduced in

P. stutzeri RCH2 strain JWST9066 (*ΔpurU*) (Supplemental Fig. S05). *P. stutzeri* RCH2 strain JWST9063 (*ΔuraD*) accumulated allantoin, presumably from spontaneous conversion of 2-oxo-4-hydroxy-4-carboxy-5-ureidoimidazoline (OHCU) to (R)-allantoin, which RCH2 would be unable to use in downstream nitrogen assimilation pathways without a racemase (46), an enzyme *P. stutzeri* has been shown to lack (47). *P. stutzeri* RCH2 strain JWST9060 (*ΔproA*) and *P. stutzeri* RCH2 strain JWST9069 (*ΔproB*), both known auxotrophs for proline (48), had reduced consumption of glutamate (precursor in proline synthesis) from N1B4, when compared to wild-type (Supplemental Fig. S05).

DISCUSSION

Biofilm formation and morphology in pseudomonas appears to be regulated by a combination of biotic factors including, but not limited to: phenazines, exopolysaccharide production, signaling molecules and flagellar activity (49). In pigmented species of pseudomonas, it has been shown that a reduced cytoplasm (induced under anoxic and low nitrate conditions) as measured by NADH:NAD+ ratio results in a rugose or wrinkled morphology while under aerobic and normal nitrate conditions, where reduction of phenazines or nitrate to dinitrogen gas occurs, they maintain a smooth morphology (50). Interestingly, *P. stutzeri*, has a distinguishing morphological characteristic of forming rugose or wrinkled colonies following initial isolation and culture on agar. While brown in color due to cytochrome c, they are classified as a nonpigmented, nonfluorescent pseudomonas and are not known to produce phenazines(13). *P. stutzeri* can grow anaerobically in the presence of nitrate and has been used for denitrification purposes(13). However, it has been demonstrated that after repeated culture, smooth colonies can form and it may take several transfers in nitrate media under semi-aerobic conditions before they are able to grow under denitrifying anaerobic conditions (13).

Four genes important for survival of *P. stutzeri RCH2* on the surface of *P. fluorescens* FW300-N1B4 were evaluated for their effects on utilization of metabolites from N1B4. From metabolomics analysis, we

have postulated possible metabolic interactions that may support the growth of RCH2. Given that PurU is important in maintenance of one carbon pools, the *ΔpurU* mutant may be unable to obtain the reaction products (THF and formate) from N1B4, and as suggested by previous studies in *E. coli,* may experience glycine starvation due to GlyA inhibition by methionine and adenine (metabolites present in N1B4 spent medium) (51). In some bacterial species, the ureide pathway is utilized for recovery of nitrogen from purines under stress conditions(52, 53). Under aerobic conditions or presence of ammonia, N2 fixation in *P. stutzeri* is suppressed and nitrification is active, however in biofilm, nitrogen fixation is suspected to occur in the EPS sacs produced by the rugose morphology(45, 54). At the N1B4 – RCH2 interface of the co-colony (which lacked EPS sacs in imaging) and in liquid culture with shaking and sufficient gas exchange, nitrogen fixation may be suppressed in favor of utilization of exchanged organic nitrogen compounds / intermediate allantoin precursors (5-hydroxyisouric acid or OHCU) from N1B4 spend medium, prior to conversion to usable (S)-allantoin. The wild-type may use exchanged glutamate for proline synthesis while the proline synthesis mutants are likely unable to obtain enough proline directly from N1B4 and is likely unable to sufficiently utilize alternative sources such peptide degradation or by alternative synthesis from ornithine (Supplemental Fig. S05). Together, these results indicate the growth of the RCH2 may be reliant upon uptake of metabolites produced by the N1B4.

While our experiments focused on cooperative interactions, inhibitory interactions may be of interest in controlling pathogenic strains in agricultural systems. The inhibitory interactions of certain pseudomonas species have been studied in detail. For example, some pathogenic species of pseudomonads produce lipodepsipeptides (e.g.. corpeptins from *P. corrugata*, a plant pathogen) which also have antimicrobial activity (55). These may contribute to interspecific competition between pseudomonads by inhibiting biofilm formation and breaking down existing biofilm (56). An interesting follow up study involving a mutant library of *Pseudomonas corrugate N2F2*, may elucidate the mechanism of inhibition between the two species and the nature of its competitive and pathogenic

behavior in nature. Additionally, some beneficial strains such as *P. aureofaciens*, an anti-fungal symbiont of wheat, releases phenazines in the rhizosphere which inhibit the growth of plant pathogens in response to exogenously diffusible signaling molecules (57). These compounds may contribute to competitiveness and the ability to form biofilms (58). Interestingly, phenazines may have multiple functional roles (59), including involvement of the redox state of the cytoplasm (50, 60); interactions such as these may be important determinants of co-colony biofilm structure under varying oxygenic conditions.

In this work we have demonstrated that bacterial printing can be used to rapidly screen for macroscopic interactions such as changes to colony morphology, size and color. We take advantage of a mutant fitness library and metabolomics to gain insights into genes and compounds mediating observed bacterial interactions. We anticipate that this approach integrating bacterial printing, mutant fitness libraries, targeted genetics, and metabolomics is suitable to investigating diverse microbial interactions. In some instances cooperative growth may be favorable (such as for bioremediation purposes where both consortia and biofilm based systems are used). In other cases, competitive interactions may be desired for biocontrol based purposes or for understanding competitive interactions in soil environments. Knowledge of the genomic and metabolic determinants involved in these interactions allows for more directed design of co-colony based systems and a better understanding of those existing in nature. We foresee BIMA becoming a valuable tool for the enhancement and understanding of *P. stutzeri* and other co-colony based systems.

Acknowledgements

Study design, sample collection, data analysis and interpretation, and manuscript preparation by ENIGMA (Ecosystems and Networks Integrated with Genes and Molecular Assemblies, http://enigma.lbl.gov, a Scientific Focus Area Program at Lawrence Berkeley National Laboratory), is

supported by the U.S. Department of Energy, Office of Science, Office of Biological & Environmental Research, Genomic Sciences Program under contract number DE-AC02-05CH11231 to Lawrence Berkeley National Laboratory. Data analysis used resources of the National Energy Research Scientific Computing Center, a Department of Energy Office of Science User Facility operated under contract number DE-AC02-05CH11231. The funders had no role in study design, data collection and interpretation, or the decision to submit the work for publication.

References

1. Louie KB, Bowen BP, Cheng X, Berleman JE, Chakraborty R, Deutschbauer A, Arkin A, Northen TR. 2013. “Replica-Extraction-Transfer” Nanostructure-Initiator Mass Spectrometry Imaging of Acoustically Printed Bacteria. Anal Chem 85:10856–10862.

2. Goodman AL, Wu M, Gordon JI. 2011. Identifying microbial fitness determinants by insertion sequencing using genome-wide transposon mutant libraries. Nat Protoc 6:1969–1980.

3. Kosina SM, Danielewicz MA, Mohammed M, Ray J, Suh Y, Yilmaz S, Singh AK, Arkin AP, Deutschbauer AM, Northen TR. 2016. Exometabolomics Assisted Design and Validation of Synthetic Obligate Mutualism. ACS Synth Biol 5:569–576.

4. Wetmore KM, Price MN, Waters RJ, Lamson JS, He J, Hoover CA, Blow MJ, Bristow J, Butland G, Arkin AP, Deutschbauer A. 2015. Rapid quantification of mutant fitness in diverse bacteria by sequencing randomly bar-coded transposons. MBio 6:e00306-15.

5. Price MN, Wetmore KM, Waters RJ, Callaghan M, Ray J, Liu H, Kuehl JV, Melnyk RA, Lamson JS, Suh Y, Carlson HK, Esquivel Z, Sadeeshkumar H, Chakraborty R, Zane GM, Rubin BE, Wall JD, Visel A, Bristow J, Blow MJ, Arkin AP, Deutschbauer AM. 2018. Mutant phenotypes for thousands of bacterial genes of unknown function. Nature 557:503–509.

394 6. Baran R, Reindl W, Northen TR. 2009. Mass spectrometry based metabolomics and enzymatic
395 assays for functional genomics. Curr Opin Microbiol 12:547–552.

396 7. Silby MW, Winstanley C, Godfrey S a. C, Levy SB, Jackson RW. 2011. Pseudomonas genomes:
397 Diverse and adaptable. FEMS Microbiol Rev 35:652–680.

398 8. Peix A, Ramírez-Bahena MH, Velázquez E. 2009. Historical evolution and current status of the
399 taxonomy of genus Pseudomonas. Infect Genet Evol 9:1132–1147.

400 9. Sørensen J, Nybroe O. 2004. Pseudomonas in the Soil Environment, p. 369–401. *In* Ramos, J-L (ed.),
401 Pseudomonas: Volume 1 Genomics, Life Style and Molecular Architecture. Springer US, Boston, MA.

402 10. Li L, Abu Al-Soud W, Bergmark L, Riber L, Hansen LH, Magid J, Sørensen SJ. 2013. Investigating the
403 diversity of pseudomonas spp. in soil using culture dependent and independent techniques. Curr
404 Microbiol 67:423–430.

405 11. Garbeva P, Van Veen JA, Van Elsas JD. 2004. Assessment of the diversity, and antagonism towards
406 Rhizoctonia solani AG3, of Pseudomonas species in soil from different agricultural regimes. FEMS
407 Microbiol Ecol 47:51–64.

408 12. Moore ERB, Tindall BJ, Dos Santos VAPM, Pieper DH, Ramos J-L, Palleroni NJ. 2006. Nonmedical:
409 Pseudomonas. The Prokaryotes.

410 13. Lalucat J, Bennasar A, Bosch R, García-Valdés E, Palleroni NJ. 2006. Biology of Pseudomonas
411 stutzeri. Microbiol Mol Biol Rev 70:510–547.

412 14. Jiang Q, Zhou C, Wang Y, Si F, Zhou Y, Chen B, Zhao Y, Chen J, Xiao M. 2014. Pseudomonas stutzeri
413 strain possessing a self-transmissible TOL-like plasmid degrades phenol and promotes maize
414 growth in contaminated environments. Appl Biochem Biotechnol 172:3461–3475.

15. Sepúlveda-Torre L, Huang A, Kim H, Criddle CS. 2002. Analysis of regulatory elements and genes required for carbon tetrachloride degradation in Pseudomonas stutzeri strain KC. J Mol Microbiol Biotechnol 4:151–161.

16. Han R, Qin L, Brown ST, Christensen JN, Beller HR. 2012. Differential isotopic fractionation during Cr(VI) reduction by an aquifer-derived bacterium under aerobic versus denitrifying conditions. Appl Environ Microbiol 78:2462–2464.

17. Moscoso F, Deive FJ, Longo M a., Sanromán M a. 2012. Technoeconomic assessment of phenanthrene degradation by Pseudomonas stutzeri CECT 930 in a batch bioreactor. Bioresour Technol 104:81–89.

18. Kaczorek E, Jesionowski T, Giec A, Olszanowski A. 2012. Cell surface properties of Pseudomonas stutzeri in the process of diesel oil biodegradation. Biotechnol Lett 34:857–862.

19. Gałazka A, Król M, Perzyński A. 2012. The efficiency of rhizosphere bioremediation with Azospirillum sp. and pseudomonas stutzeri in soils freshly contaminated with PAHs and diesel fuel. Pol J Environ Stud 21:345–353.

20. Nguyen PD, Van Ginkel CG, Plugge CM. 2008. Anaerobic degradation of long-chain alkylamines by a denitrifying Pseudomonas stutzeri. FEMS Microbiol Ecol 66:136–142.

21. Brodie EL, Joyner DC, Faybishenko B, Conrad ME, Rios-Velazquez C, Malave J, Martinez R, Mork B, Willett A, Koenigsberg S, Herman DJ, Firestone MK, Hazen TC. 2011. Microbial community response to addition of polylactate compounds to stimulate hexavalent chromium reduction in groundwater. Chemosphere 85:660–665.

22. Liu D, Zhang S, Zheng Y, Shoun H. 2006. Denitrification by the mix-culturing of fungi and bacteria

436 with shell. Microbiol Res 161:132–137.

437 23. Clarens M, Bernet N, Delgenès JP, Moletta R. 1998. Effects of nitrogen oxides and denitrification by
438 Pseudomonas stutzeri on acetotrophic methanogenesis by Methanosarcina mazei. FEMS Microbiol
439 Ecol 25:271–276.

440 24. Erna NM, Banerjee S, Khatoon H, Shariff M, Yusoff FMD. 2013. Immobilized Nitrifying Bacterial
441 Consortium for Improving Water Quality , Survival and Growth of Penaeus monodon Fabricius 1798
442 Postlarvae in Hatchery System. Asian Fish Sci 26:212–221.

443 25. Deng B, Fu L, Zhang X, Zheng J, Peng L, Sun J, Zhu H, Wang Y, Li W, Wu X, Wu D. 2014. The
444 Denitrification Characteristics of Pseudomonas stutzeri SC221-M and Its Application to Water
445 Quality Control in Grass Carp Aquaculture. PLoS One 9:e114886.

446 26. Shen X, Hu H, Peng H, Wang W, Zhang X. 2013. Comparative genomic analysis of four
447 representative plant growth-promoting rhizobacteria in Pseudomonas. BMC Genomics 14:271.

448 27. Cottyn B, Debode J, Regalado E, Mew TW, Swings J. 2009. Phenotypic and genetic diversity of rice
449 seed-associated bacteria and their role in pathogenicity and biological control. J Appl Microbiol
450 107:885–897.

451 28. Miyahara M, Kim S-W, Zhou S, Fushinobu S, Yamada T, Ikeda-Ohtsubo W, Watanabe A, Miyauchi K,
452 Endo G, Wakagi T, Shoun H. 2012. Survival of the Aerobic Denitrifier Pseudomonas stutzeri Strain
453 TR2 during Co-Culture with Activated Sludge under Denitrifying Conditions. Biosci Biotechnol
454 Biochem 76:495–500.

455 29. Moscoso F, Deive FJ, Villar P, Pena R, Herrero L, Longo M a., Sanromán M a. 2012. Assessment of a
456 process to degrade metal working fluids using Pseudomonas stutzeri CECT 930 and indigenous

457 microbial consortia. Chemosphere 86:420–426.

458 30. Badar U, Shoeb E, Qureshi FM, Akhtar J, Ahmed N. 2013. Removal of Copper Via Bioreactor By Soil
459 Isolate. Academic Research International 4:253–259.

460 31. Lazarova VZ, Capdeville B, Nikolov L. 1992. Biofilm Performance of a Fluidized Bed Biofilm Reactor
461 for Drinking Water Denitrification. Water Sci Technol 26:555–566.

462 32. Zhao Y, Qu D, Zhou R, Yang S, Ren H. 2016. Efficacy of forming biofilms by Pseudomonas migulae
463 AN-1 toward in situ bioremediation of aniline-contaminated aquifer by groundwater circulation
464 wells. Environmental Science and Pollution Research.

465 33. Viggiani A, Olivieri G, Siani L, Di Donato A, Marzocchella A, Salatino P, Barbieri P, Galli E. 2006. An
466 airlift biofilm reactor for the biodegradation of phenol by Pseudomonas stutzeri OX1. J Biotechnol
467 123:464–477.

468 34. Han R, Geller JT, Yang L, Brodie EL, Chakraborty R, Larsen JT, Beller HR. 2010. Physiological and
469 transcriptional studies of Cr(VI) reduction under aerobic and denitrifying conditions by an aquifer-
470 derived pseudomonad. Environ Sci Technol 44:7491–7497.

471 35. Schneider CA, Rasband WS, Eliceiri KW. 2012. NIH Image to ImageJ: 25 years of image analysis. Nat
472 Methods 9:671–675.

473 36. R Core Team. 2014. R: A Language and Environment for Statistical Computing. R Foundation for
474 Statistical Computing, Vienna, Austria.

475 37. Hothorn T, Bretz F, Westfall P. 2008. Simultaneous inference in general parametric models. Biom J
476 50:346–363.

38. Vaccaro BJ, Lancaster WA, Thorgersen MP, Zane GM, Younkin AD, Kazakov AE, Wetmore KM, Deutschbauer A, Arkin AP, Novichkov PS, Wall JD, Adams MWW. 2016. Novel Metal Cation Resistance Systems from Mutant Fitness Analysis of Denitrifying Pseudomonas stutzeri. Appl Environ Microbiol 82:6046–6056.

39. Horton RM, Cai ZL, Ho SN, Pease LR. 1990. Gene splicing by overlap extension: tailor-made genes using the polymerase chain reaction. Biotechniques 8:528–535.

40. Chakraborty R, Woo H, Dehal P, Walker R, Zemla M, Auer M, Goodwin LA, Kazakov A, Novichkov P, Arkin AP, Hazen TC. 2017. Complete genome sequence of Pseudomonas stutzeri strain RCH2 isolated from a Hexavalent Chromium [Cr(VI)] contaminated site. Stand Genomic Sci 12:23.

41. Li MZ, Elledge SJ. 2007. Harnessing homologous recombination in vitro to generate recombinant DNA via SLIC. Nat Methods 4:251–256.

42. Fels SR, Zane GM, Blake SM, Wall JD. 2013. Rapid transposon liquid enrichment sequencing (TnLE-seq) for gene fitness evaluation in underdeveloped bacterial systems. Appl Environ Microbiol 79:7510–7517.

43. Yao Y, Sun T, Wang T, Ruebel O, Northen T, Bowen BP. 2015. Analysis of Metabolomics Datasets with High-Performance Computing and Metabolite Atlases. Metabolites 5:431–442.

44. Bowen BP, Northen TR. 2010. Dealing with the unknown: metabolomics and metabolite atlases. J Am Soc Mass Spectrom 21:1471–1476.

45. Wang D, Xu A, Elmerich C, Ma LZ. 2017. Biofilm formation enables free-living nitrogen-fixing rhizobacteria to fix nitrogen under aerobic conditions. ISME J 11:1602–1613.

46. Bovigny C, Degiacomi MT, Lemmin T, Peraro MD, Stenta M. 2014. Reaction Mechanism and

498 Catalytic Fingerprint of Allantoin Racemase. The Journal of Physical Chemistry B.

499 47. Van Der Drift L, Vogels GD, Van Der Drift C. 1975. Allantoin racemase: A new enzyme from
500 Pseudomonas species. Biochimica et Biophysica Acta (BBA) - Enzymology 391:240–248.

501 48. http://fit.genomics.lbl.gov/; accessed 05/14/2020.

502 49. Merritt JH, Ha DG, Cowles KN, Lu W, Morales DK, Rabinowitz J, Gitai Z, O'Toole GA. 2010. Specific
503 control of Pseudomonas aeruginosa surface-associated behaviors by two c-di-GMP diguanylate
504 cyclases. MBio 1.

505 50. Dietrich LEP, Okegbe C, Price-Whelan A, Sakhtah H, Hunter RC, Newmana DK. 2013. Bacterial
506 community morphogenesis is intimately linked to the intracellular redox state. J Bacteriol
507 195:1371–1380.

508 51. Nagy PL, Marolewski A, Benkovic SJ, Zalkin H. 1995. Formyltetrahydrofolate hydrolase, a regulatory
509 enzyme that functions to balance pools of tetrahydrofolate and one-carbon tetrahydrofolate
510 adducts in Escherichia coli. J Bacteriol 177:1292–1298.

511 52. Serventi F, Ramazzina I, Lamberto I, Puggioni V, Gatti R, Percudani R. 2010. Chemical basis of
512 nitrogen recovery through the ureide pathway: formation and hydrolysis of S-ureidoglycine in
513 plants and bacteria. ACS Chem Biol 5:203–214.

514 53. Izaguirre-Mayoral ML, Lazarovits G, Baral B. 2018. Ureide metabolism in plant-associated bacteria:
515 purine plant-bacteria interactive scenarios under nitrogen deficiency. Plant Soil 428:1–34.

516 54. Yan Y, Ping S, Peng J, Han Y, Li L, Yang J, Dou Y, Li Y, Fan H, Fan Y, Li D, Zhan Y, Chen M, Lu W, Zhang
517 W, Cheng Q, Jin Q, Lin M. 2010. Global transcriptional analysis of nitrogen fixation and ammonium
518 repression in root-associated Pseudomonas stutzeri A1501. BMC Genomics 11:11.

519 55. Raaijmakers JM, de Bruijn I, Nybroe O, Ongena M. 2010. Natural functions of lipopeptides from
520 Bacillus and Pseudomonas: More than surfactants and antibiotics. FEMS Microbiol Rev 34:1037–
521 1062.

522 56. Kuiper I, Lagendijk EL, Pickford R, Derrick JP, Lamers GEM, Thomas-Oates JE, Lugtenberg BJJ,
523 Bloemberg GV. 2004. Characterization of two Pseudomonas putida lipopeptide biosurfactants,
524 putisolvin I and II, which inhibit biofilm formation and break down existing biofilms. Mol Microbiol
525 51:97–113.

526 57. Pierson LS, Pierson E a. 1996. Phenazine antibiotic production in Pseudomonas aureofaciens: Role
527 in rhizosphere ecology and pathogen suppression. FEMS Microbiol Lett 136:101–108.

528 58. Ramos I, Dietrich LEP, Price-Whelan A, Newman DK. 2010. Phenazines affect biofilm formation by
529 Pseudomonas aeruginosa in similar ways at various scales. Res Microbiol 161:187–191.

530 59. Mavrodi DV, Blankenfeldt W, Thomashow LS. 2006. Phenazine compounds in fluorescent
531 Pseudomonas spp. biosynthesis and regulation. Annu Rev Phytopathol 44:417–445.

532 60. Glasser NR, Kern SE, Newman DK. 2014. Phenazine redox cycling enhances anaerobic survival in
533 Pseudomonas aeruginosa by facilitating generation of ATP and a proton-motive force. Mol
534 Microbiol 92:399–412.

535

536 Figure legends

537 **Fig. 1 Biofilm Interaction Mapping and Analysis (MIMA) of the biochemical and biophysical**
538 **interactions required for co-colony fitness.** (A) An acoustic printer or automated liquid handling system
539 is used to print underlay colonies of different strains spaced apart to reduce interactions and a single

strain grid of overlay colonies to evaluate the macroscopic interactions of the co-colony formation including: inhibition of colonization, direct overlay growth, morphology, color and motility. (B) Transmission electron microscopy is used to evaluate the interface between the two co-colony strains and the changes over time. (C) Mutant fitness profiling of a DNA-barcoded transposon mutant library of the overlay colony allows for investigation of genes important for co-colony formation and fitness. (D) Mass spectrometry based metabolomics is used to analyze the metabolites consumed/released in the co-culture versus mono-culture.

Figure 2. Colony interaction screening. (A) Fourteen Pseudomonas "effector" strains (spots #1-14) and one uninoculated control medium (spot #15) were printed from liquid cultures onto an agar plate (blue). After 2 days of incubation, the interaction strain, *P. stutzeri* RCH2 (#1) was printed in all other positions (white). (B) Image taken at 6 days total incubation time indicated inhibited growth of *P. stutzeri* RCH2 around strains 1 (self), 3, 4, 5, 6, 7, 8, 9 and 11. (C and D) *P. stutzeri* RCH2, the interaction strain, colony size was used to evaluate which effector strains had a significant (ANOVA, Dunnett's test, $p<0.001$ ***, $p<0.01$ **, $p< 0.05$ *) effect on the growth of the neighboring RCH2 colonies. One effector strain (#2), N1B4, with the largest mean colony area and not inhibited by RCH2, was selected for further morphological and metabolic interaction with RCH2. When comparing all surrounding colonies, only 7 was significantly different from control (Supplemental fig. S2).

Figure. 3 Transmission electron microscopy of co-colony morphology. (A) Timepoint images of a co-colony of *Pseudomonas* sp. FW300-N1B4 (underlay) and *Pseudomonas stutzeri* RCH2 (overlay) were taken every 6 hours for the first 24 hours of the overlay culture. Control N1B4 cultures remain smooth (see Fig. 4 and S02). (B) Transmission electron microscopy imaging (1400x) of vertical slices showing the co-colony structure, air-colony interface, and strain interface were taken at 2, 12 and 24 hours of aerobic RCH2 overlay culture, and at 24 hours of an anaerobic RCH2 overlay culture. Similar imaging at

563 24 hours of aerobic RCH2 and N1B4 monocultures were used to determine staining and morphology of
564 each cell type.

565 **Figure 4. RCH2 mutant co-colony interactions.** (A) RB-TnSeq mutant library fitness assay, (B) mutant
566 growth on N1B4 spent and fresh media, (C) mutant growth on N1B4 colonies. All strains of RCH2 grew
567 alone (on control sterile medium underlay) and formed rugose colonies by 24 hours of overlay culture
568 (Supplemental Fig. S3, Supplemental Table S5). Images are notated with "S" or "R" for smooth or rugose
569 morphology, respectively; location noted when rugose morphology was located only in the center or
570 periphery of the colony.

571 **Fig. 5 Metabolomics.** N1B4 spent medium was sterile filtered and used to culture *Pseudomonas stutzeri*
572 RCH2 wild-type, and mutants *ΔuraD*, *ΔpurU*, *ΔproA*, *ΔproB* for 24 hours before collection of extracellular
573 metabolites for extraction and LCMS analysis. A media control was incubated alongside the sample
574 cultures to control for contamination and for comparison with starting metabolite abundances. A
575 targeted analysis was performed using a library of m/z, retention time and MS2 spectra of common
576 polar metabolites. Metabolites with significantly different abundances relative to control media
577 (ANOVA, Tukey HSD, $p<0.05$) are indicated with an asterisk. Metabolites with significantly different
578 abundance between at least two of the cultures are indicated with #. Boxplots and statistical
579 comparisons are available in Supplemental Figure S4, S5 and Table S6.

580

581

1. Screening

Biofilm Interactions

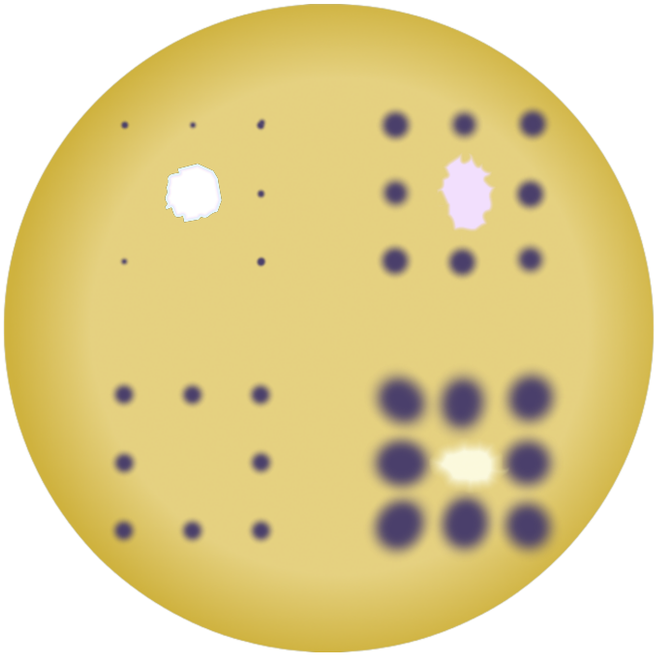

2. Morphology

Co-colony Interface

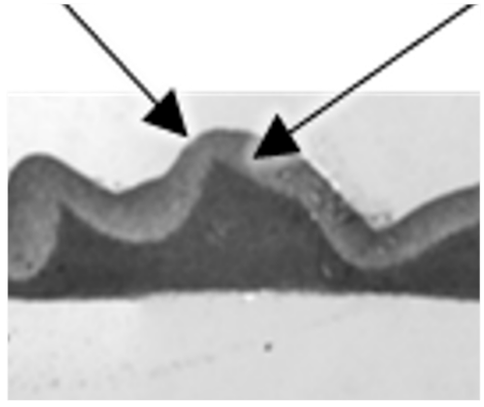

3. Genomics

Mutant Fitness & Interaction

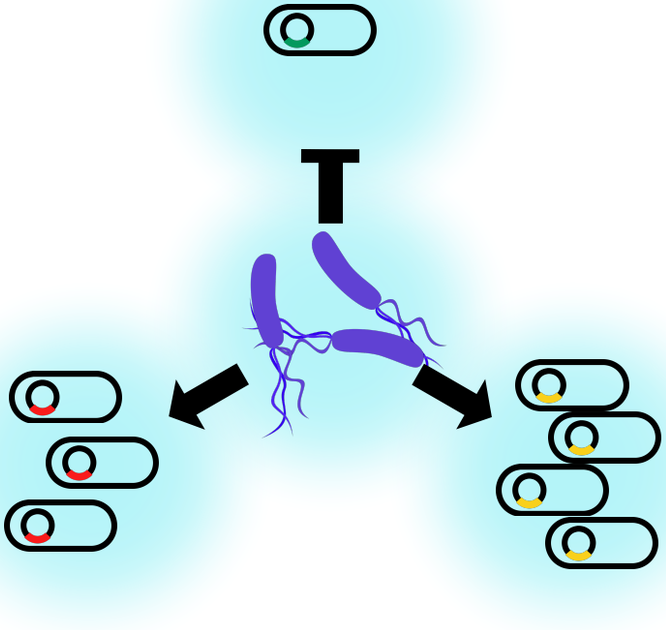

4. Metabolomics

Nutrient Dynamics & Exchange

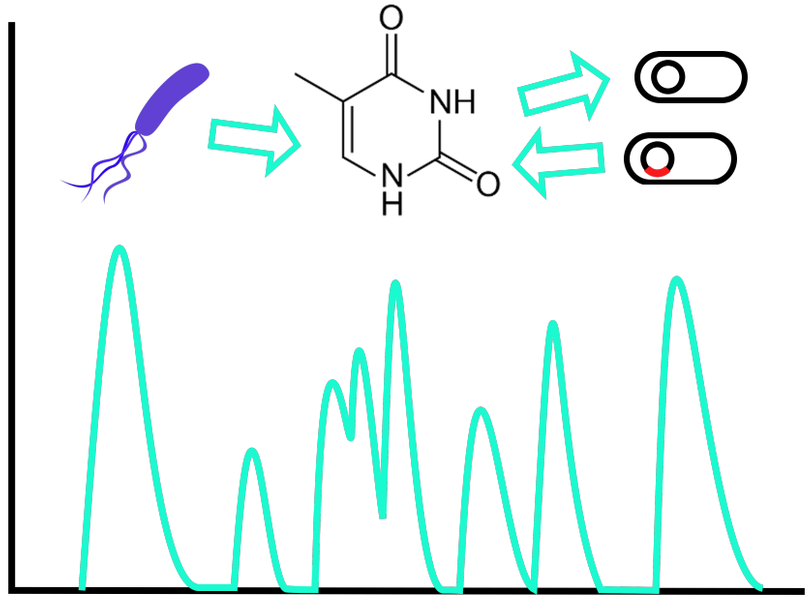

	1	2	3	4	5	6	7	8	9	10	11	12	13	14	15	16	17	18	19	20	21	22	23	24
1	1	1	1	1	1	1	1	1	1	1	1	1	1	1	1	1	1	1	1	1	1	1	1	1
2	1	1	1	1	1	1	1	1	1	1	1	1	1	1	1	1	1	1	1	1	1	1	1	1
3	1	1	1	1	1	1	1	1	1	1	1	1	1	1	1	1	1	1	1	1	1	1	1	1
4	1	1	1	1	1	1	1	2	1	1	1	3	1	1	1	4	1	1	1	5	1	1	1	1
5	1	1	1	1	x	1	1	1	1	1	1	1	1	1	1	1	1	1	1	1	1	1	1	1
6	1	1	1	1	1	1	1	1	1	1	1	1	1	1	1	1	1	1	1	1	1	1	1	1
7	1	1	1	1	1	1	1	1	1	1	1	1	1	1	1	1	1	1	1	1	1	1	1	1
8	1	1	1	6	1	1	1	7	1	1	1	8	1	1	1	9	1	1	1	10	1	1	1	1
9	1	1	1	1	1	1	1	1	1	1	1	1	1	1	1	1	1	1	1	1	1	1	1	1
10	1	1	1	1	1	1	1	1	1	1	1	1	1	1	1	1	1	1	1	1	1	1	1	1
11	1	1	1	1	1	1	1	1	1	1	1	1	1	1	1	1	1	1	1	1	1	1	1	1
12	1	1	1	11	1	1	1	12	1	1	1	13	1	1	1	14	1	1	1	15	1	1	1	1
13	1	1	1	1	1	1	1	1	1	1	1	1	1	1	1	1	1	1	1	1	1	1	1	1
14	1	1	1	1	1	1	1	1	1	1	1	1	1	1	1	1	1	1	1	1	1	1	1	1
15	1	1	1	1	1	1	1	1	1	1	1	1	1	1	1	1	1	1	1	1	1	1	1	1
16	1	1	1	1	1	1	1	1	1	1	1	1	1	1	1	1	1	1	1	1	1	1	1	1

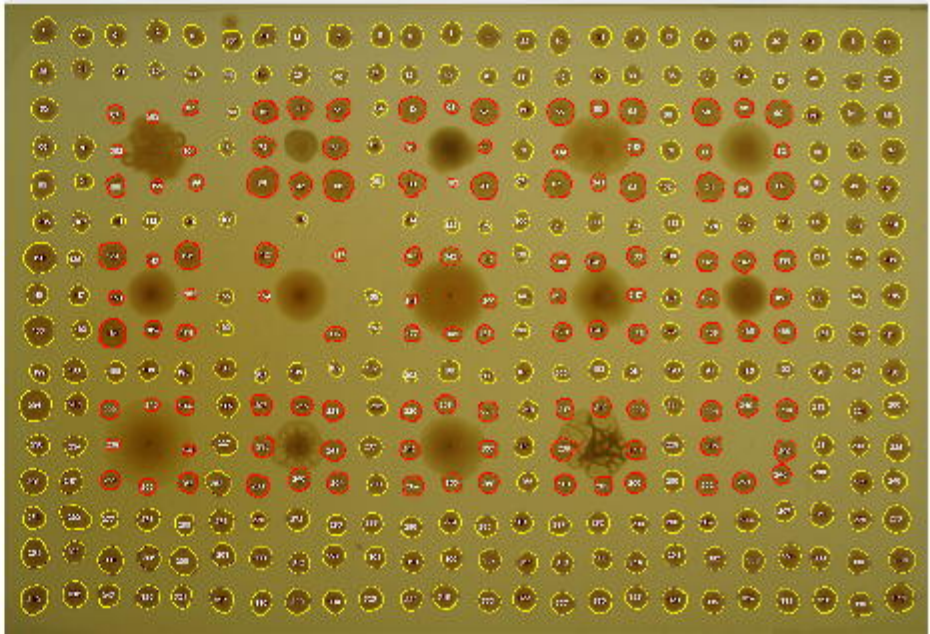

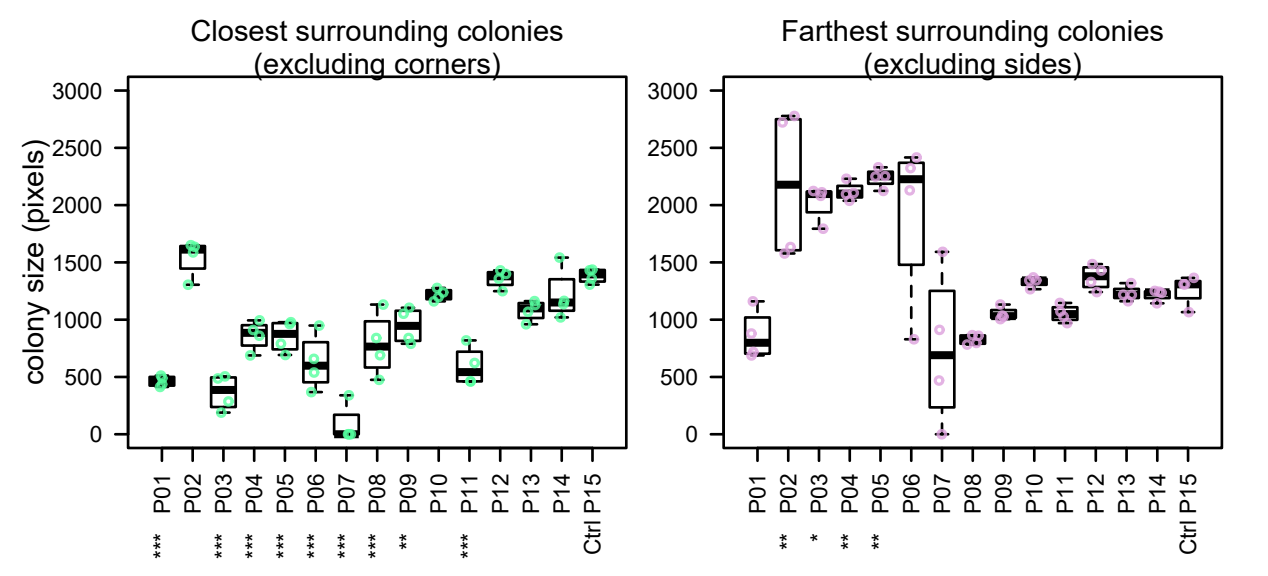
Closest surrounding colonies
(excluding corners)
Farthest surrounding colonies
(excluding sides)
colony size (pixels)
0
500
1000
1500
2000
2500
3000
P01
P02
P03
P04
P05
P06
P07
P08
P09
P10
P11
P12
P13
P14
Ctrl P15
*** *** *** *** *** *** ** *** **
** * ** **

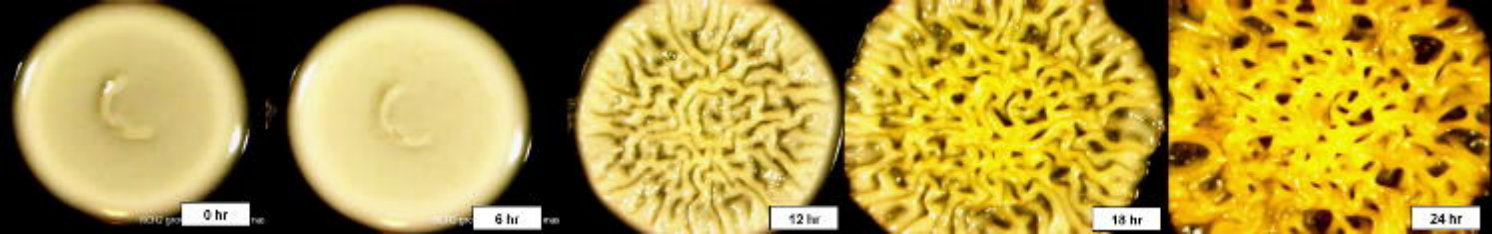
0 hr
6 hr
12 hr
18 hr
24 hr

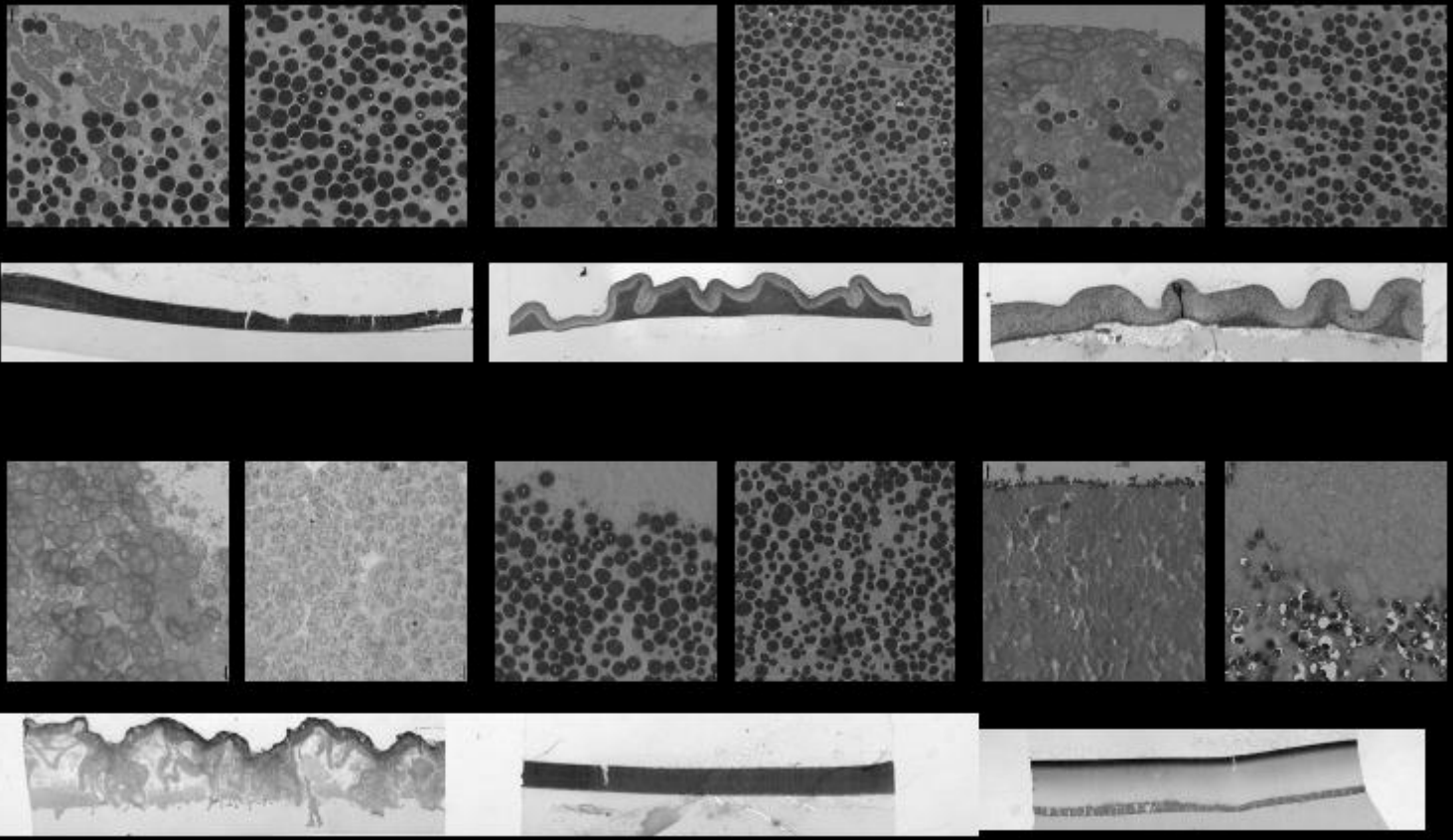

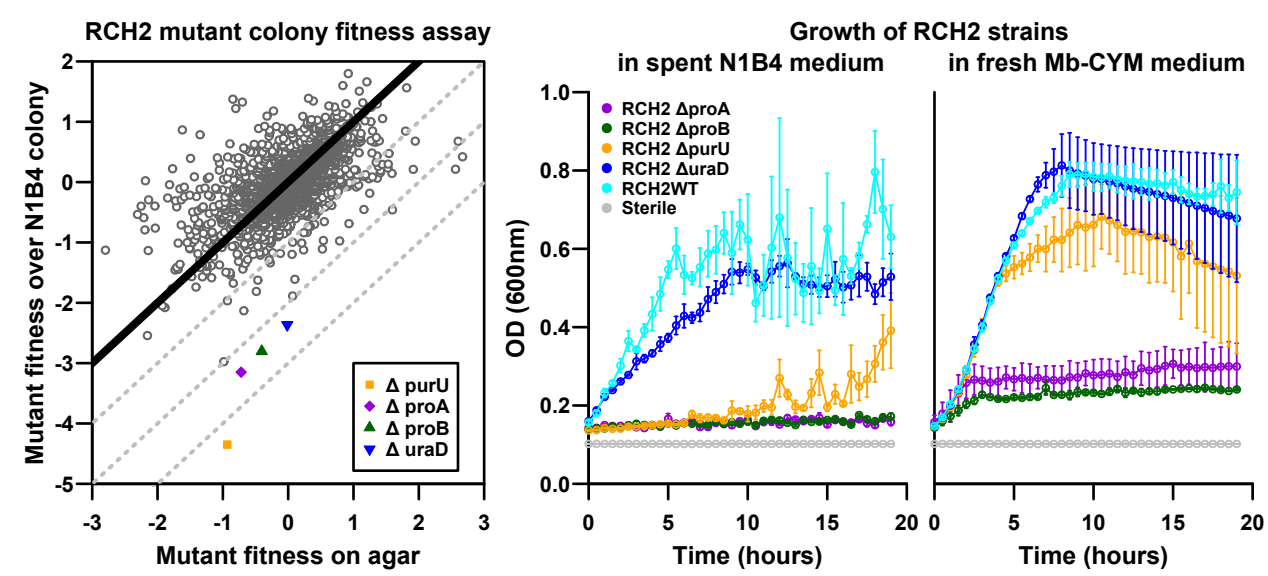
RCH2 mutant colony fitness assay
Mutant fitness over N1B4 colony
Mutant fitness on agar
Δ purU
Δ proA
Δ proB
Δ uraD
Growth of RCH2 strains
in spent N1B4 medium
in fresh Mb-CYM medium
OD (600nm)
RCH2 ΔproA
RCH2 ΔproB
RCH2 ΔpurU
RCH2 ΔuraD
RCH2WT
Sterile
Time (hours)
Time (hours)

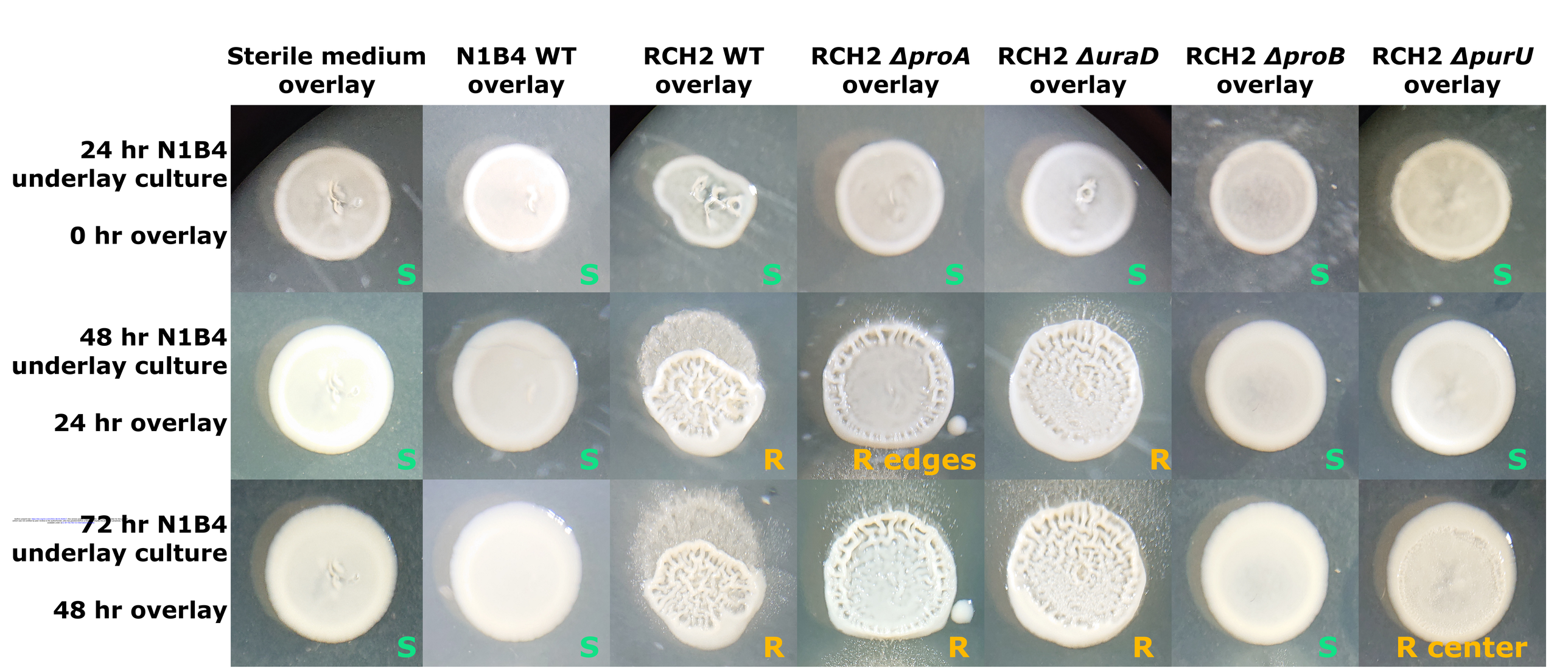
Sterile medium overlay
N1B4 WT overlay
RCH2 WT overlay
RCH2 ΔproA overlay
RCH2 ΔuraD overlay
RCH2 ΔproB overlay
RCH2 ΔpurU overlay
24 hr N1B4 underlay culture
0 hr overlay
48 hr N1B4 underlay culture
24 hr overlay
72 hr N1B4 underlay culture
48 hr overlay
S
S
S
S
S
S
S
S
S
R
R edges
R
S
S
S
S
R
R
R
S
R center

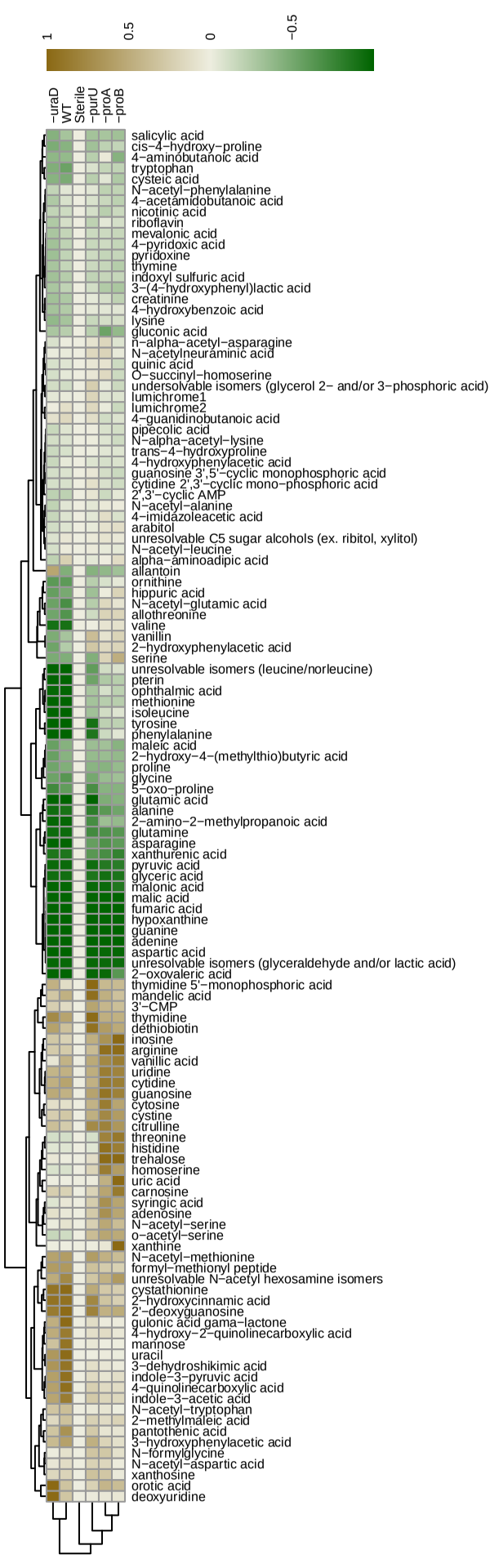
1
0.5
0
−0.5
−uraD
WT
Sterile
−purU
−proA
−proB
salicylic acid
cis−4−hydroxy−proline
4−aminobutanoic acid
tryptophan
cysteic acid
N−acetyl−phenylalanine
4−acetamidobutanoic acid
nicotinic acid
riboflavin
mevalonic acid
4−pyridoxic acid
pyridoxine
thymine
indoxyl sulfuric acid
3−(4−hydroxyphenyl)lactic acid
creatinine
4−hydroxybenzoic acid
lysine
gluconic acid
n−alpha−acetyl−asparagine
N−acetylneuraminic acid
quinic acid
O−succinyl−homoserine
undersolvable isomers (glycerol 2− and/or 3−phosphoric acid)
lumichrome1
lumichrome2
4−guanidinobutanoic acid
pipecolic acid
N−alpha−acetyl−lysine
trans−4−hydroxyproline
4−hydroxyphenylacetic acid
guanosine 3',5'−cyclic monophosphoric acid
cytidine 2',3'−cyclic mono−phosphoric acid
2',3'−cyclic AMP
N−acetyl−alanine
4−imidazoleacetic acid
arabitol
unresolvable C5 sugar alcohols (ex. ribitol, xylitol)
N−acetyl−leucine
alpha−aminoadipic acid
allantoin
ornithine
hippuric acid
N−acetyl−glutamic acid
allothreonine
valine
vanillin
2−hydroxyphenylacetic acid
serine
unresolvable isomers (leucine/norleucine)
pterin
ophthalmic acid
methionine
isoleucine
tyrosine
phenylalanine
maleic acid
2−hydroxy−4−(methylthio)butyric acid
proline
glycine
5−oxo−proline
glutamic acid
alanine
2−amino−2−methylpropanoic acid
glutamine
asparagine
xanthurenic acid
pyruvic acid
glyceric acid
malonic acid
malic acid
fumaric acid
hypoxanthine
guanine
adenine
aspartic acid
unresolvable isomers (glyceraldehyde and/or lactic acid)
2−oxovaleric acid
thymidine 5'−monophosphoric acid
mandelic acid
3'−CMP
thymidine
dethiobiotin
inosine
arginine
vanillic acid
uridine
cytidine
guanosine
cytosine
cystine
citrulline
threonine
histidine
trehalose
homoserine
uric acid
carnosine
syringic acid
adenosine
N−acetyl−serine
o−acetyl−serine
xanthine
N−acetyl−methionine
formyl−methionyl peptide
unresolvable N−acetyl hexosamine isomers
cystathionine
2−hydroxycinnamic acid
2'−deoxyguanosine
gulonic acid gama−lactone
4−hydroxy−2−quinolinecarboxylic acid
mannose
uracil
3−dehydroshikimic acid
indole−3−pyruvic acid
4−quinolinecarboxylic acid
indole−3−acetic acid
N−acetyl−tryptophan
2−methylmaleic acid
pantothenic acid
3−hydroxyphenylacetic acid
N−formylglycine
N−acetyl−aspartic acid
xanthosine
orotic acid
deoxyuridine